Int. J. Electrochem. Sci., 13 **(2018)** 6708 – 6716, doi: 10.20964/2018.07.54

International Journal of
ELECTROCHEMICAL
SCIENCE
www.electrochemsci.org

Hydrothermal Synthesis and Electrochemical Properties of MoS_2/C Nanocomposite

Haishen Song[1,2,3,], Anping Tang[1], Guorong Xu[2], Lihua Liu[3], Yijin Pan[2], and Mengjia Yin[2]*

[1] Key Laboratory of Theoretical Organic Chemistry and Functional Molecule, Ministry of Education
[2] School of Chemistry and Chemical Engineering, Hunan University of Science and Technology, Xiangtan 411201, PR China
[3] Hunan Provincial Key Laboratory of Controllable Preparation and Functional Application of Fine Polymers, Hunan Province College Key Laboratory of QSAR/QSPR
[*]E-mail: Song_shs@126.com

Received: 16 March 2018 / *Accepted:* 12 April 2018 / *Published:* 5 June 2018

A molybdenum disulfide/carbon (MoS_2/C) nanocomposite was synthesized by a simple hydrothermal method using glucose as a carbon source followed by carbonization. The sample was systematically investigated by using X-ray diffraction (XRD), field-emission scanning electron microscopy (FESEM) and high-resolution transmission electron microscopy (HRTEM). Electrochemical performances were evaluated in two-electrode cells versus metallic sodium. The synthesized MoS_2/C composite exhibits an initial capacity of 475.1 mAh g^{-1} at a current density of 100 mA g^{-1}, and a capacity retention of 71% is obtained after 100 cycles at a current density of 250 mA g^{-1}. The material shows enhanced electrochemical performances compared with pristine MoS_2 due to incorporation of the conductive carbon, which suppressed significant volumetric change in MoS_2 during the charge/discharge process and increased the electrical conductivity of MoS_2.

Keywords: MoS_2/C composite; hydrothermal synthesis; anode material; sodium-ion battery

1. INTRODUCTION

Due to the wide availability and low cost of sodium, sodium-ion batteries (SIBs) have attracted considerable attention in recent years as promising alternatives to lithium ion batteries[1-4]. Although the intercalation mechanism of sodium is very similar to that of lithium, the larger ion radius and transport barrier restrict the choice of electrode materials for SIBs[5,6]. Therefore, it is of great importance to explore a suitable host for SIBs.

Transition metal dichalcogenides (MX_2) with a similar feature of layered structure as graphite have great potential as alternative anode materials for sodium ion storage[7-10]. Over the past few years, great attention has been paid to molybdenum disulfide (MoS_2) due to its high theoretical specific

capacity and good cycling performance in sodium storage[11-13]. MoS_2 has a similar layered structure as graphite in which each layer has a slab of transition metal atoms sandwiched by two slabs of chalcogenide atoms. In the structure, adjacent MoS_2 layers are interconnected with weak van der Waals forces, and there is sufficient space between the layers to host sodium ions[14,15]. These structural features ensure fast intercalation and deintercalation of Na^+ between the MoS_2 planes, which suggests the possibility of MoS_2 as a potential electrode material for high capacity rechargeable batteries. However, the electronic and ionic conductivity between two contiguous S-Mo-S layers is unsatisfactory, and the material suffers from large volume expansion and pulverization when used as an anode material, which leads to poor cycle performance and poor rate capability[7,12]. Efforts have been made to circumvent these drawbacks and improve its electrochemical properties[16-20]. One of the effective approaches to overcome these problems is to design composites with a matrix that can enhance the electronic and ionic conductivity and act as a buffer layer for the volume expansion during charge-discharge processes[21,22]. Among those materials, MoS_2-carbon composite is the most promising candidate as a high-performance, stable anode for sodium ion batteries.

We previously reported that molybdenum disulfide/reduced graphene oxide (MoS_2/RGO) showed excellent electrochemical properties as an anode material for sodium ion batteries compared with pristine MoS_2[23]. To improve the electrochemical performances of MoS_2 and accelerate both electron and ion transport in a simpler way, a MoS_2/C composite has been prepared in this paper by a hydrothermal method using glucose as a carbon source. The results demonstrated that the obtained MoS_2/C composite shows enhanced electrochemical performances due to incorporation of the conductive carbon. An initial capacity of 475.1 mAh g^{-1} is obtained at a current density of 100 mA g^{-1}, and the composite maintains 71% of initial capacity after 100 cycles at a current density of 250 mA g^{-1}.

2. EXPERIMENTAL SECTION

2.1 Synthesis of the MoS_2/C composites

MoS_2/C composite was synthesized via the followed procedure: 1.5 g of sodium molybdate, 1.9 g of thiourea and 1.0 g of glucose were dispersed in 60 ml of ultrapure water under vigorous stirring to form a homogeneous solution. After stirring for 20 min, the solution was transferred into a 100-ml Teflon-lined stainless steel autoclave, sealed tightly, and hydrothermally treated in an electric oven at 180 ℃ for 24 h. After cooling naturally, the resulting black precipitate was collected by filtering and washing with ultrapure water and absolute ethanol several times and dried at 80 ℃ in a vacuum for 12 h. Then, this precipitate was calcined at 800 ℃ for 2 h under argon atmosphere at a heating rate of 2 ℃ min^{-1}. For comparison, pure MoS_2 was synthesized through similar procedures without adding glucose and further calcination.

2.2 Material characterization

An X-ray diffractometer (Bruker D-8) (Cu Kα, l=0.154056 nm) was applied to study the phase structure of the samples. Field emission scanning electron microscopy (JSM-6360LV, JEOL) and

high-resolution transmission electron microscopy (Tecnai G2F20 S-TWIX) were used to determine the morphology of the as-prepared composites. Raman spectra (LabRAM HR800) were obtained with a laser excitation of 532 nm.

2.3 Electrochemical measurements

The electrochemical properties were studied by using two-electrode cells that were assembled in an argon-filled glove box. The electrodes were fabricated by mixing active material, acetylene black and sodium alginate (7:2:1 wt/wt/wt) in water to form a uniform slurry. Then, it was coated on copper foils and subsequently dried in a vacuum oven at 80 ℃ overnight. The CR2032 coin cells were assembled in an argon-filled glove box using a glass microfiber (Whatman) membrane and sodium metal foil as the separator and counter electrode, respectively. The electrolyte was a mixture of 1 M $NaClO_4$ in EC/DMC (1:1, vl/vl) with 5 wt% fluoroethylene carbonate (FEC). Galvanostatic charge/discharge measurements were carried out in the voltage range of 0.01~3.00 V on a battery tester at various current densities. Cyclic voltammetry (CV) measurements were performed on an electrochemical workstation within the voltage range of 0.01~3.00 V at a scan rate of 0.2 mV s^{-1}. Electrochemical impedance spectroscopy (EIS) was conducted by applying a 5 mV amplitude signal in the frequency range of 100 kHz to 0.01 Hz. The specific capacity of the electrode was calculated based on the total mass of MoS_2/C synthesized in the experiment.

3. RESULTS AND DISCUSSION

The morphologies of the pristine MoS_2 and MoS_2/C composite were characterized using TEM and SEM, which are shown in Figure 1. It can be seen from Figure 1a and Figure 1b that MoS_2 appears as a flower-like particle structure composed of wrinkled nanosheets. After the addition of carbon, MoS_2 particles were coated with a carbon layer with some tiny curled nanosheets on its surface, and the nanosheets stretched out towards the edges.

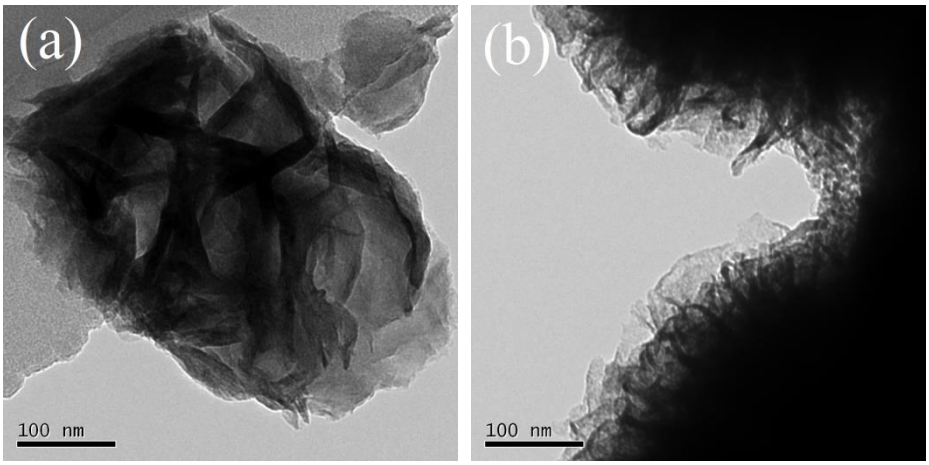

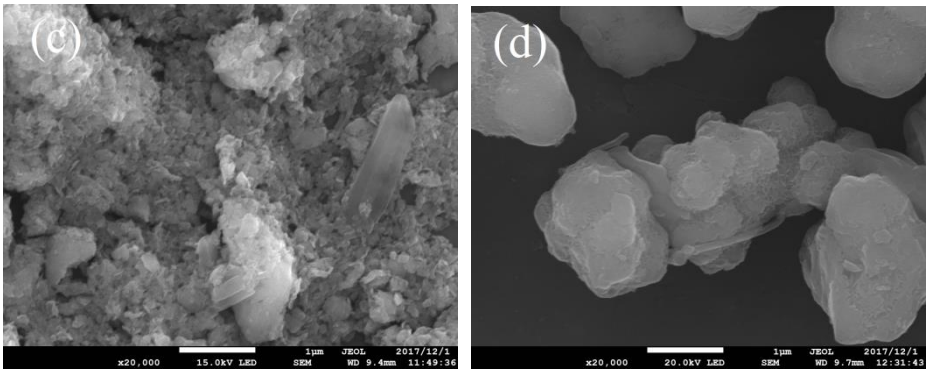

Figure 1. TEM images of MoS_2 (a) and MoS_2/C (b); SEM images of MoS_2 (c) and MoS_2/C (d)

Figure 1c and Figure 1d show typical SEM images of bare MoS_2 and the MoS_2/C composite. It reveals that bare MoS_2 obtained through the proposed method aggregates severely, and they are randomly assembled into a stacked structure. In addition, the MoS_2/C composite displays a loose structure consisting of a large number of scaled sheets. Moreover, the as-prepared MoS_2/C sample exhibits spherical morphologies, and these microspheres are not completely separate from each other but often coupled together.

The XRD patterns of pure MoS_2 and MoS_2/C are presented in Figure 2. As shown in the Figure, MoS_2 exhibits high crystallinity, and the diffraction peaks observed at 14.1°, 33.3°, 44.4° and 58.65° correspond to different crystal planes of hexagonal MoS_2, which is in accordance with those established by JCPDS card number 37-1492[24,25,26]. The strong peak at 14.1° corresponds to the (002) plane with a d-spacing of 0.63 nm, indicating that layered MoS_2 grows well along the c axis during synthesis. No obvious difference is observed from the diffraction patterns of MoS_2 and MoS_2/C, indicating that the introduction of glucose in the synthesis process does not change the phase of MoS_2 and that the coated carbon possesses an amorphous character[27,28].

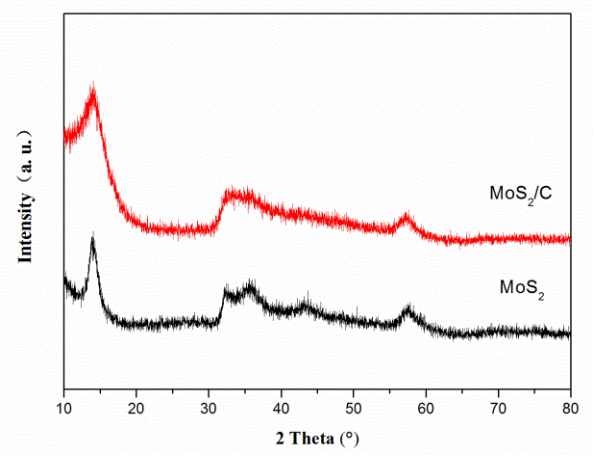

Figure 2. X-ray diffraction patterns of MoS_2 and MoS_2/C

Raman spectroscopy is used to study the structures of MoS_2 and MoS_2/C (Figure 3). Both MoS_2 and MoS_2/C exhibit two typical peaks at approximately 375 cm^{-1} and 405 cm^{-1}, corresponding to A_{1g} and E_{2g} modes of the hexagonal MoS_2 crystal, respectively. The E_{2g} mode refers to the in-layer

displacement of Mo and S atoms, whereas the A_{1g} mode refers to the out-of-layer symmetric displacements of S atoms along the c axis[28]. The frequency difference between E_{2g} and A_{1g} can provide the layer-thickness information of MoS_2 based materials. The frequency difference for the MoS_2/C sample is 24.9 cm^{-1}, compared with 26.4 cm^{-1} for the pure MoS_2 sample. The decrease in frequency difference suggests that the MoS_2/C composite has a thinner layer structure than pure MoS_2, which will increase the surface area of the material and the contact area between the electrolyte and electrode material[29]. There are two other distinct peaks at approximately 1360 cm^{-1} and 1590 cm^{-1} in the Raman spectra of MoS_2/C, demonstrating the existence of carbon in MoS_2/C. Meanwhile, the wide diffraction peak in the MoS_2 spectrum at about 1590 cm^{-1} may come from carbon residue in thiourea, which is in good accordance with the synthesis process.

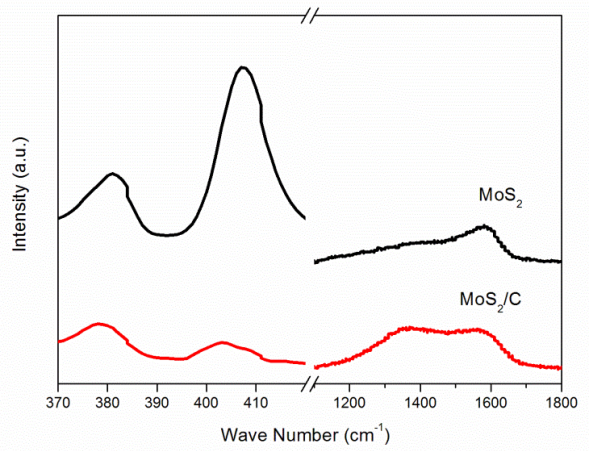

Figure 3. Raman spectra of MoS_2 and MoS_2/C

Figure 4 shows the typical cyclic voltammetry curves of MoS_2/C composite and pure MoS_2. As displayed in Figure 4a, the prominent cathodic peak located at approximately 0.90 V in the first cycle corresponds to the insertion of Na^+ into MoS_2 and formation of the SEI (solid electrolyte interphase) layer. The peak located at approximately 0.1 V corresponds to the formation of Mo and Na_2S. The anodic peak located at approximately 1.8 V is due to the oxidation reaction from Mo to MoS_2[7]. In the subsequent cycles, the former cathodic peak disappears, and two new peaks centred at approximately 1.4 V and 0.7 V arise. These new cathodic peaks coupled with anodic peaks are related to the Na_2S/S reversible redox reactions and sodium storage on the boundaries or interface of the Mo/Na_2S_x composites[30,31]. The anodic curves during subsequent cycles show similar characteristics to that of the first cycle, while the cathodic curves show differences, which can be attributed to the formation of an SEI film in the first cycle. After the second cycle, the CV curves are almost overlapped, suggesting that the electrochemical properties are stabilized in subsequent cycles after the 2nd cycle. The MoS_2 electrode exhibits a similar CV profile as the MoS_2/C electrode, as shown in Figure 4b.

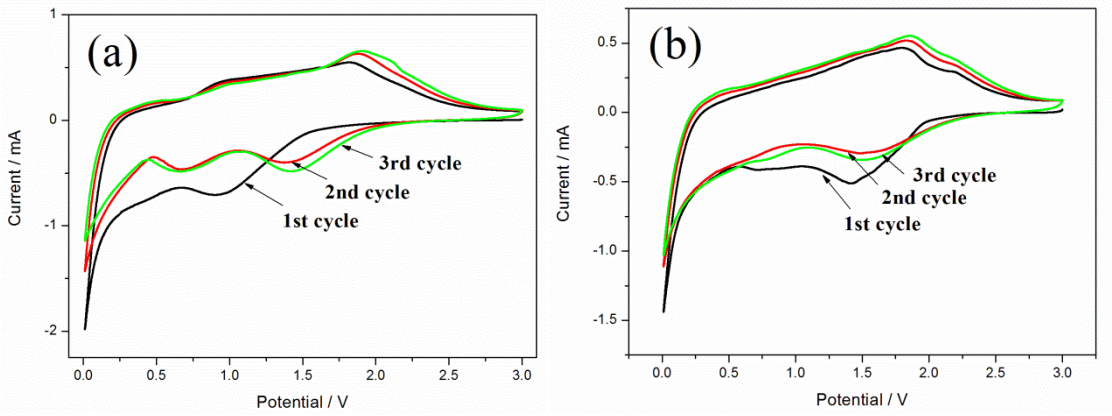

Figure 4. Cyclic voltammetry curves of MoS_2/C (a) and MoS_2 (b) at a scan rate of 0.2 mV s^{-1}

Figure 5 illustrates the first three charge and discharge curves of the synthesized MoS_2/C composite and pure MoS_2 at a current density of 100 mA g^{-1}. A sloping plateau starting from 1.5 to 1.0 V and a flat plateau at approximately 0.2 V were observed for MoS_2/C in the first discharge process (Figure 5a). This is consistent with the 1st cathodic sweep of the CV curve in Figure 4a. The potential variation in the sodium intercalation can be attributed to the insertion of additional Na^+ ions into the expanded MoS_2 structure or in the defect sites of MoS_2. During the charge process, the sloping plateau starting from approximately 1.2 V corresponds to the anodic peak at 1.8 V of the CV curves. The MoS_2 electrode shows a similar charge-discharge profile, which manifests the fact that the coated carbon layer did not change the sodium storage mechanism of MoS_2. The MoS_2/C electrode delivers a specific capacity of 475.1 mAh g^{-1} in the first charge process, and the capacity of the MoS_2 electrode is 470.0 mAh g^{-1}. The capacity of the MoS_2/C composite is slightly higher than that of the pure MoS_2, primarily due to the increased surface area of MoS_2/C and thus more active sites for the insertion/extraction of Na^+ ions.

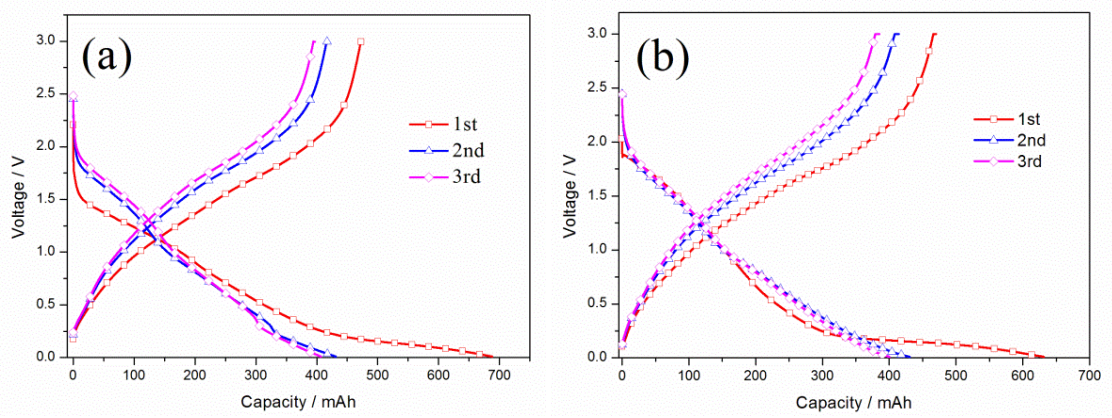

Figure 5. First three charge and discharge curves of MoS_2/C (a) and MoS_2 (b) at a current density of 100 mA g^{-1}

The cycling performances of MoS_2 and MoS_2/C are tested at a current density of 250 mA g^{-1}. Figure 6a shows that the MoS_2 electrode suffers from a poor cycling performance, and the capacity

quickly decreased to 125 mAh g^{-1} after 100 cycles. In contrast, the addition of carbon improves the cycling stability of the material, and MoS_2/C exhibits a better capacity retention of more than 71% compared with 39.6% for MoS_2, which is consistent with former studies[27,28]. This improved cycling performance can be ascribed to the interconnected conductive carbon network, which suppresses the large volumetric change in MoS_2 during the charge/discharge process and increases the electrical conductivity of MoS_2. In addition, the increased surface area of MoS_2/C offers more active sites for electrochemical reactions and increases the contact area between the electrolyte and electrode material, which is also beneficial for improving the electrochemical performances.

To better understand the electrochemical kinetics of MoS_2 and MoS_2/C, EIS measurements were carried out. The obtained impedance spectra as shown in Figure 6b consist of mainly two parts: a semi-circular arc at middle frequencies and a sloped-line-like diffusion behaviour at low frequencies. Generally, the depressed semi-circular arc at the middle frequencies is related to the capacitive behaviour with a parallel resistance on the electrode/electrolyte interface, for instance, a double-layer capacitance with a parallel charge transfer resistance and capacitance of an SEI layer in parallel with its resistance. In addition, the inclined line corresponds to a sodium-diffusion process within the bulk of the electrode material[23,28]. The middle-frequency arc width values significantly decrease with the addition of carbon, which can be interpreted as a decrease in the interfacial resistance that is induced by the convenient charge transition on the MoS_2/C anode. This fact confirms that the incorporation of carbon can preserve the high conductivity of the MoS_2/C composite electrode and enhance rapid electron transport during the electrochemical sodium insertion/extraction reaction, resulting in improved electrochemical performances, which is in good accordance with the charge/discharge performances.

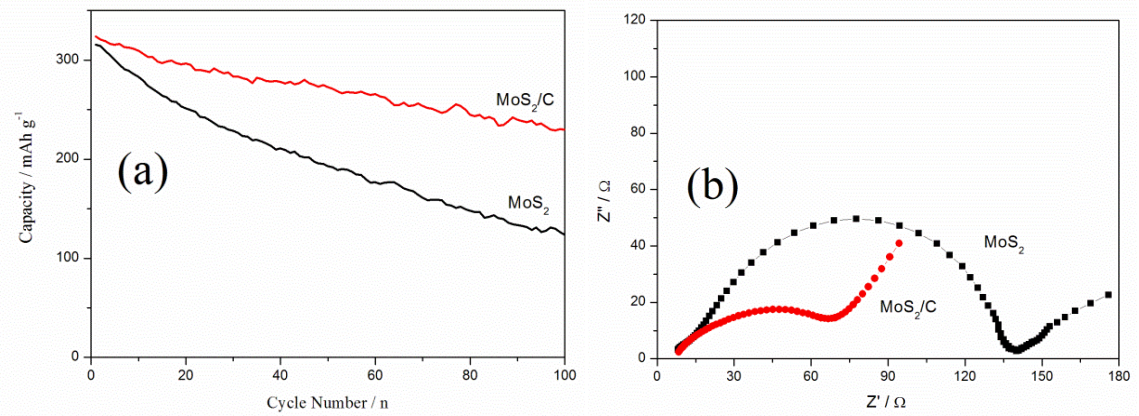

Figure 6. Cycling behaviours of MoS_2 and MoS_2/C at a current density of 250 mA g^{-1} (a) and Nyquist plots of MoS_2 and MoS_2/C (b)

4. CONCLUSIONS

Nanostructured MoS_2/C composite with a flower-like morphology was synthesized through a facile hydrothermal route using glucose as a carbon source and was utilized as the electrode material of

a sodium ion battery. The MoS_2/C composite exhibits spherical morphologies with some tiny curled nanosheets on its surface, and the addition of carbon inhibits the aggregation of MoS_2 nanosheets. In addition, the incorporation of conductive carbon suppresses significant volumetric change in MoS_2 and greatly enhances rapid electron transport during the sodium insertion/extraction reaction, thus resulting in an improvement in electrochemical performances. Therefore, the MoS_2/C composite presents an improved capacity of 475.1 mAh g^{-1} and a capacity retention of 71% after 100 cycles at a current density of 250 mA g^{-1} compared with only 39.6% for MoS_2.

ACKNOWLEDGEMENTS
This work was supported by the Natural Science Foundation of Hunan Province, China (2018JJ3176), and the Research Foundation of Education Bureau of Hunan Province, China (15C0532).

References

1. C. Nithya and S. Gopukumar, *Wiley interdisciplinary reviews: Energy and environment*, 4(2015)253.
2. N. Yabuuchi, K. Kubota, M. Dahbi and S. Komaba, *Chem. Rev.*, 114(2014)11636.
3. P. Vassilaras, S. T. Dacek, H. Kim, T. T. Fister, S. Kim, G. Ceder and J. C. Kim, *J. Electrochem. Soc.*, 164(2017)A3484.
4. Y. Xie, H. C. Wang, R. Liu, Z. G. Wang, W. Wen, Z. Jiang, Z. L. Gong and Y. Yang, *J. Electrochem. Soc.*, 164(2017)A3487.
5. S. W. Kim, D. H. Seo, X. H. Ma, G. Ceder and K. Kang, *Adv. Energy Mater.*, 2(2012)710.
6. H. Su, S. Jaffer and H. J. Yu, *Energy Storage Materials*, 5(2016)116.
7. P. Zhang, F. R. Qin, L. Zou, M. R. Wang, K. Zhang, Y. Q. Lai and J. Li, *Nanoscale*, 9(2017)2189.
8. S. H. Choi and Y. C. Kang, *Nanoscale*, 7(2015)3965.
9. H. Wang, X. Z. Lan, D. L. Jiang, Y. Zhang, H. H. Zhong, Z. P. Zhang and Y. Jiang, *J. Power Sources*, 283(2015)187.
10. Z. Hu, L. X. Wang, K. Zhang, J. B. Wang, F. Y. Cheng, Z. L. Tao and J. Chen, *Angew. Chem.*, 126(2014)13008.
11. L. David, R. Bhandavat and G. Singh, *ACS Nano*, 8(2014)1759.
12. Q. Q. Li, Z. P. Yao, J. S. Wu, S. Mitra, S. Q. Hao, T. S. Sahu, Y. Li, C. Wolverton and V. P. Dravid, *Nano Energy*, 38(2017)342.
13. X. Huang, Z. Zeng and H. Zhang, *Chem. Soc. Rev.*, 42(2013)1934.
14. W. Xu, T. Wang, S. D. Wu and S. Wang, *J. Alloy. Compd.*, 698(2017)68.
15. A.V. Murugan, M. Quintin, M.H. Delville, G. Campet, C. S. Gopinath and K. Vijayamohanan, *J. Power Sources*, 156(2006)615.
16. B. Ahmed, D. H. Anjum, M. N. Hedhili and H. N. Alshareef, *Small*, 11(2015)4341.
17. D. B. Xiao, J. Y. Zhang, X. Li, D. Zhao, H. Y. Huang, J. L. Huang, D. X. Cao, Z. H. Li and C. M. Niu, *ACS Nano*, 10(2016)9509.
18. Y. L. Jia, H. Q. Wan, L. Chen, H. D. Zhou and J. M. Chen, *J. Power Sources*, 354 (2017)1.
19. Y. Yuan, F.F. Huang, A.Q. Pan and W. Xiao, *Int. J. Electrochem. Sci.*, 12(2017)5431.
20. S. Li, Zhigao Luo, X.X. Cao, G.Z. Fang and S.Q. Liang, *Int. J. Electrochem. Sci.*, 13(2018)23.
21. K. Chang and W. X. Chen, *ACS Nano*, 5(2011)4720.
22. X. Zhang, X. Li, J. Liang, Y. Zhu and Y. Qian, *Small*, 12(2016)2484.
23. H. S. Song, A. P. Tang, G. R. Xu, L. H. Liu, M. J. Yin and Y. J. Pan, *Int. J. Electrochem. Sci.*, 13(2018)4720.
24. H. S. S. Ramakrishna Matte, A. Gomathi, A. K. Manna, D.J. Late, R. Datta, S. K. Pati and C. N. R.

Rao, *Angew. Chem.*, 122(2010)4153.
25. K. Chang, Z. W. Mei, T. Wang, Q. Kang, S. X. Ouyang and J. H. Ye, *ACS Nano*, 8(2014)7078.
26. Y. R. Cui, J. S. He, X. M. Li, J. X. Zhao, A. L. Chen and J. Yang, *Adv. Mater. Res.*, 631(2013)306.
27. Q. Jiang, X. Chen, L. Li, C. Q. Feng and Z. P. Guo, *J. Electron. Mater.*, 46(2017)1079.
28. Y. Liu, D. P. Tang, H. X. Zhong, Q. Y. Zhang, J. W. Yang and L. Z. Zhang, *J. Alloy. Compd.*, 729(2017)583.
29. R. T. Wang, S. H. Wang, D. D. Jin, Y. B. Zhang, Y. J. Cai, J. M. Ma and L. Zhang, *Energy Storage Materials*, 9(2017)195.
30. S. D. Lacey, J. Wan, A. v. W. Cresce, S. M. Russell, J. Dai, W. Bao, K. Xu and L. Hu, *Nano Lett.*, 15(2015)1018.
31. J. Wang, C. Luo, T. Gao, A. Langrock, A. C. Mignerey and C. Wang, *Small*, 11(2015)473.